Cell Reports

Resource

Human Organ Chip Models Recapitulate Orthotopic Lung Cancer Growth, Therapeutic Responses, and Tumor Dormancy In Vitro

Graphical Abstract

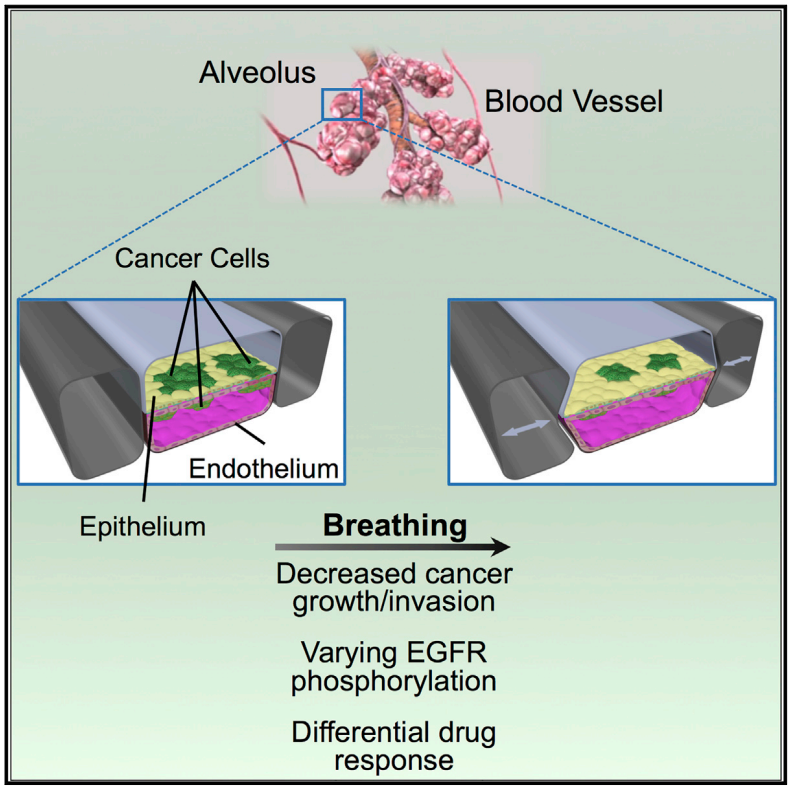

Authors

Bryan A. Hassell, Girija Goyal, Esak Lee, Alexandra Sontheimer-Phelps, Oren Levy, Christopher S. Chen, Donald E. Ingber

Correspondence

don.ingber@wyss.harvard.edu

In Brief

Hassell et al. demonstrate that, when human lung cancer cells are grown within organ-on-a-chip culture devices that mimic lung structure and function, tumor cells recapitulate tumor growth and invasion patterns, as well as responses to therapy, observed in human patients. They also discover that breathing motions influence these responses.

Highlights

- Organ-on-a-chip technology recapitulates human cancer growth and invasion patterns
- Physiological breathing motions suppress cancer cell growth and invasion
- Tumor cells become resistant to drug therapy with breathing motions
- This model permits analysis of cancer persister cells in vitro

Hassell et al., 2017, Cell Reports *21*, 508–516
October 10, 2017
https://doi.org/10.1016/j.celrep.2017.09.043

CellPress

OPEN ACCESS
CellPress

Cell Reports
Resource

Human Organ Chip Models Recapitulate Orthotopic Lung Cancer Growth, Therapeutic Responses, and Tumor Dormancy In Vitro

Bryan A. Hassell,[1,2] Girija Goyal,[1] Esak Lee,[1,3] Alexandra Sontheimer-Phelps,[1,4] Oren Levy,[1] Christopher S. Chen,[1,3] and Donald E. Ingber[1,2,5,6,*]

[1]Wyss Institute for Biologically Inspired Engineering at Harvard University, Boston, MA 02115, USA
[2]Harvard John A. Paulson School of Engineering and Applied Sciences, Cambridge, MA 02139, USA
[3]Department of Biomedical Engineering and the Biological Design Center, Boston University, Boston, MA 02215, USA
[4]Department of Biology, University of Freiburg, Freiburg, Germany
[5]Vascular Biology Program and Department of Surgery, Boston Children's Hospital and Harvard Medical School, Boston, MA 02115, USA
[6]Lead Contact
*Correspondence: don.ingber@wyss.harvard.edu
https://doi.org/10.1016/j.celrep.2017.09.043

SUMMARY

Here, we show that microfluidic organ-on-a-chip (organ chip) cell culture technology can be used to create in vitro human orthotopic models of non-small-cell lung cancer (NSCLC) that recapitulate organ microenvironment-specific cancer growth, tumor dormancy, and responses to tyrosine kinase inhibitor (TKI) therapy observed in human patients in vivo. Use of the mechanical actuation functionalities of this technology revealed a previously unknown sensitivity of lung cancer cell growth, invasion, and TKI therapeutic responses to physical cues associated with breathing motions, which appear to be mediated by changes in signaling through epidermal growth factor receptor (EGFR) and MET protein kinase. These findings might help to explain the high level of resistance to therapy in cancer patients with minimal residual disease in regions of the lung that remain functionally aerated and mobile, in addition to providing an experimental model to study cancer persister cells and mechanisms of tumor dormancy in vitro.

INTRODUCTION

Development of improved cancer therapeutics requires better experimental models (Hackam and Redelmeier, 2006). To meet this challenge, animal researchers have moved away from conventional subcutaneous implants because they do not mimic organ-specific differences in cancer growth or responses to therapy observed in patients (Fidler et al., 1994). Instead, human tumor xenografts are often implanted in mice at the "orthotopic" organ site from which the tumors were derived (Killion et al., 1999; Gould et al., 2015). These in vivo orthotopic cancer models better mimic tumor growth and metastasis; however, when using these models, it still remains extremely difficult to identify contributions of the microenvironment to tumor growth or visualize cancer cell behaviors over time, and the organ-specific microenvironment is still not human. Thus, there has been a search for in vitro models of human cancer that might provide an alternative approach.

A key challenge in developing in vitro cancer models is that static 2D cultures primarily promote high rates of cancer cell proliferation, whereas tumors can exhibit varying levels of growth and differentiation when growing in human organs in vivo, and growth properties and drug responses can significantly differ based on the organ-specific microenvironment. As a result, most drug development programs result in discovery of therapeutics that inhibit proliferation, whereas it is extremely difficult to test for drugs that kill persister cells within dormant cancers, or tumors in different growth or differentiation states. While more complex in vitro human cancer models have been developed that permit study of various tumor responses (e.g., growth, migration, invasion, angiogenesis, extravasation, and drug effects) (Choi et al., 2015; Skardal et al., 2015; Portillo-Lara and Annabi, 2016), none of these recapitulate complex organ-level patterns of cancer growth or therapeutic responses seen in patients. We therefore set out to develop human-based in vitro orthotopic cancer models utilizing organ-on-a-chip (organ chip) technology. Organ chips are microfluidic cell culture devices created with microchip manufacturing methods that contain continuously perfused hollow microchannels inhabited by living cells arranged to simulate organ-level pathophysiology. By recapitulating the multicellular architectures, tissue-tissue interfaces, chemical gradients, mechanical cues, and vascular perfusion of the body, these devices produce levels of tissue and organ functionality not possible with conventional 2D or 3D culture systems (Bhatia and Ingber, 2014). We previously described a human lung alveolus chip containing two microfluidic channels separated by a porous extracellular matrix (ECM)-coated membrane lined on one side by human alveolar epithelial cells and pulmonary microvascular endothelium on the other, which mimics multiple normal lung functions (infection-induced recruitment of immune cells, breathing-induced absorption of nanoparticulates and associated inflammation, interleukin-2 (IL-2)-induced pulmonary edema, inflammation-induced pulmonary thrombosis, etc.) as well as response to drug therapies observed

in vivo (Huh et al., 2010, 2012; Jain et al., 2017). We also developed a similar 2-channel lung small airway chip lined by human bronchiolar epithelial cells interfaced with lung endothelium that recapitulates small airway structure and functions, including normal mucociliary clearance, cytokine production in response to infection, and changes in transcriptome when exposed to cigarette smoke (Benam et al., 2016a, 2016b).

Importantly, because these vascularized organs chips contain an endothelium-lined channel that supports dynamic fluid flow, potential therapeutics can be tested in a pharmacologically relevant context in which drugs pass through an endothelial barrier under flow, which is central to drug action as well as understanding of drug pharmacokinetics. It also provides a way to study recruitment of circulating immune cells and collect cytokines that are secreted into blood (Huh et al., 2010; Benam et al. 2016b). In addition, it is possible to flow human whole blood through the endothelium-lined channels of the lung chip (Jain et al., 2017), which could enable testing of drugs under even more physiological conditions than is possible using static culture systems (e.g., Transwells).

These lung chip models are relevant for oncology because lung cancer is the leading cause of cancer-related deaths in the United States (Siegel et al., 2017). The adenocarcinoma form of non-small-cell lung cancer (NSCLC) makes up about 40% of the approximately 150,000 yearly deaths caused by this disease (Siegel et al., 2017), and it provides an excellent example of a tumor that exhibits microenvironment-dependent differentials in growth at the organ level in that while it emerges at the bronchiolar-alveolar border of the lung, it preferentially grows along preexisting alveolar structures in human patients (Yousem and Beasley, 2007). Patients with this type of lung cancer also often have mutations in epidermal growth factor receptor (EGFR) (Pao and Chmielecki, 2010) and typically respond well to first-generation, reversible tyrosine kinase inhibitors (TKIs), although many acquire resistance and eventually require use of third-generation, irreversible TKIs (Sequist et al., 2015).

Here, we show that by orthotopically injecting a human NSCLC cell line within the primary alveolus and small airway organ chips, we were able to recapitulate organ microenvironment-specific cancer behaviors, including rampant growth in the lung alveolus microenvironment compared to relative tumor dormancy in the lung airway, as well as tumor responses to TKI therapy previously only observed in vivo. These studies not only demonstrate the feasibility of engineering in vitro *human* orthotopic cancer models with clinical relevance, but also raise the possibility that mechanical cues associated with breathing decrease lung cancer cell growth and invasion, as well as promote development of cancer persister cells that become resistant to a third-generation TKI drug.

RESULTS

Orthotopic Lung Cancer-on-a-Chip Models

To create an orthotopic model of human NSCLC representative of the in vivo microenvironment, we plated H1975 human NSCLC adenocarcinoma cells at a low cell density (3,200 cells/cm^2) simultaneously with a 100-fold higher number of *primary* lung alveolar or small airway epithelial cells on the upper surface of the ECM-coated membrane to integrate the cancer cells into the tissue layers during the tissue differentiation process (Figures 1A and 1B). After plating, the medium was removed from the upper channel to create an air-liquid interface (ALI) above the epithelium, while an ''ALI medium'' (endothelial basal medium with 0.4% serum) was continuously perfused through the lower vascular channel to feed both tissue layers. The NSCLC cells were engineered to stably express high levels of GFP to optically quantify tumor cell growth and invasion.

We took this co-plating approach to create orthotopic lung cancer chips because in our preliminary studies, we injected this number of NSCLC cells at a single site within the epithelium in airway chips after the epithelium was allowed to fully differentiate for 3 weeks at an ALI, and we found that cancer cell growth was completely inhibited, even though viable, GFP-labeled dormant tumor lesions remained present for up to 4 additional weeks of culture (Figures 1C and 1D). Furthermore, it was not possible to inject the tumor cells directly into the pre-differentiated alveolar epithelium because of the friability of this cell monolayer. Thus, we shifted to the co-culture technique.

When we analyzed the growth of the NSCLC cells that were co-cultured in the human airway chip during the differentiation process, we found that they appeared as isolated GFP-positive cells within the epithelial monolayer after tissue differentiation was completed (Figure 1E, left). Under these conditions, the lung cancer cells remained quiescent for approximately 12 days of culture on-chip before they shifted into logarithmic growth and began to exhibit a doubling time of about 40 hr (Figure 1F, top). In contrast, when these NSCLC cells were cultured on plastic culture dishes in the rich medium (DMEM with 10% serum) in which they are commonly passaged, they failed to exhibit any growth lag and proliferated even more rapidly (30 hr doubling rate) than when simultaneously plated with epithelial cells in the airway chip (Figure 1F, top). In contrast, the same tumor cells failed to exhibit any growth when cultured alone on plastic dishes in the same ALI medium used for airway chip cultures (Figure 1F, top), and thus, the engineered lung airway microenvironment clearly conveyed distinct growth signals to these cells.

Interestingly, when we co-cultured the NSCLC in the human alveolus chip, we found that they proliferated much more rapidly than when grown in the airway chip whether cultured in the presence or absence of cyclic mechanical strain (10% strain; 0.2 Hz) to mimic physiological breathing motions (Figure 1F, bottom versus top), much as is observed in human patients with this adenocarcinoma form of lung cancer in vivo (Yousem and Beasley, 2007). The growth of the cancer cells in the static alveolus chip was comparable to that observed when the cells were co-cultured with lung alveolar epithelium and endothelium in a Transwell insert even though they did not proliferate in this ALI medium on their own (Figure 1F, bottom).

We previously showed that mimicking normal breathing has potent effects on various pathophysiological responses in the human lung alveolus chip (Huh et al., 2010, 2012); however, we were surprised to find that recapitulation of this physiologically relevant mechanical microenvironment suppressed lung cancer growth significantly (by >50%; $p < 0.001$) in this model (Figures 1E, right, and 1F, bottom). When grown in the absence of

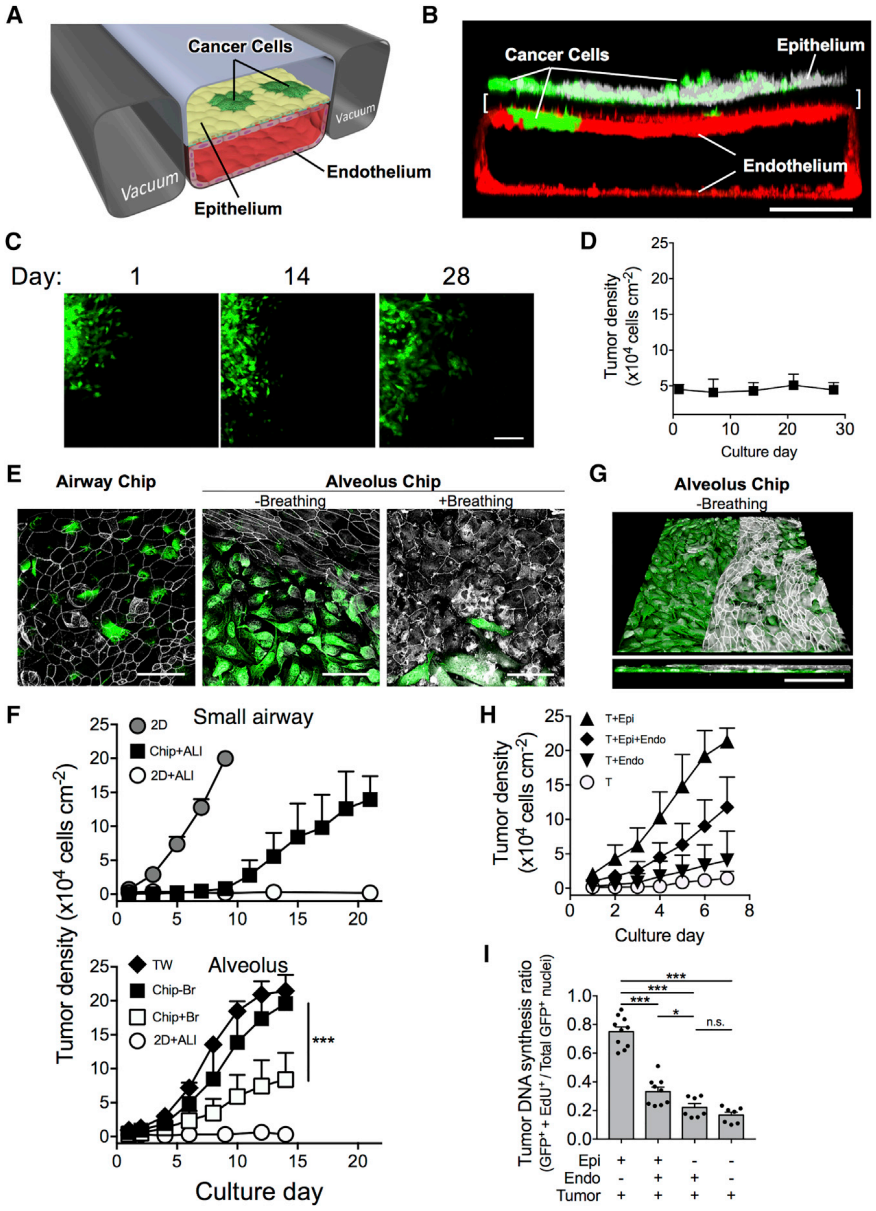

Figure 1. Human Orthotopic Lung Cancer-on-a-Chip Models

(A) Schematic diagram of a cross-section through the 2-channel microfluidic chip containing human lung epithelial cells and a low density of NSCLC tumor cells cultured on the upper surface of a porous ECM-coated membrane (brackets) with human lung microvascular endothelial cells cultured on all four walls of the lower channel, forming a hollow vascular lumen. In this schematic, the two parallel side chambers of the alveolus chip are shown; physiological breathing motions can be mimicked by applying cyclic suction to these chambers that rhythmically deform the flexible side walls and the attached horizontal membrane with the adherent lung tissues.

(B) Confocal fluorescence micrograph of a cross-section of the two central cell-lined channels of an alveolus chip, showing GFP-labeled lung cancer cells (green, anti-GFP) co-cultured with primary lung alveolar epithelial cells labeled with antibodies against the tight junction protein ZO-1 (white) at an ALI in the apical compartment of the microfluidic device. Primary lung microvascular endothelial cells labeled with anti-VE-cadherin (red) form a continuous monolayer that covers all four sides of the lower microchannel, creating a vascular lumen through which the ALI maintenance medium flows. Note that the tumor cells grow within, above, and below the epithelial monolayer, in addition to appearing within the pores of the membrane and in the endothelial monolayer below in this alveolus chip that was cultured for 7 days without breathing motions (scale bar, 200 μm).

(C) Immunofluorescence micrograph of an implanted cluster of GFP-labeled NSCLC cells (green), which do not significantly expand in number at the site of injection when viewed at 1, 14, and 28 days after implantation in the airway chip (scale bar, 100 μm).

(D) Quantification of NSCLC tumor cell densities when cultured for up to 1 month after implantation in the fully differentiated airway chip.

(E) GFP-labeled lung cancer cells (green) exhibit distinct growth patterns within the normal epithelial monolayer containing cells delineated by ZO1-containing tight junctions (white) after 2 weeks of culture in the airway chip (left) versus the alveolus chip in the absence (middle) or presence of physiological breathing motions (right) (scale bar, 50 μm).

(F) Lung cancer cell growth dynamics when cultured alone in normal growth medium in a 2D plastic dish (2D) or on the same dishes in ALI medium (2D+ALI) versus in ALI medium in the microfluidic airway chip with co-cultured normal lung small airway epithelium and endothelium (Chip+ALI) (top). lung cancer cell growth dynamics in ALI medium when cultured alone in a 2D plastic dish (2D+ALI) versus when co-cultured with normal lung alveolar epithelium and endothelium in a Transwell insert (TW) or in a microfluidic alveolus chip with (Chip+Br) or without (Chip−Br) breathing motions (bottom).

(G) Top (top) and cross-sectional (bottom) confocal fluorescence microscopic views of a non-breathing alveolus chip showing NSCLC tumor cells (green, anti-GFP) growing beneath and within the alveolar epithelium (white, anti-ZO1) and disrupting its normal epithelial continuity (scale bar, 100 μm).

(H) NSCLC tumor cell growth measured under static conditions either alone (T) or in the presence of normal lung alveolar epithelium (T+Epi), normal lung microvascular endothelium (T+Endo), or both (T+Epi+Endo).

(I) Effects on lung cancer cell DNA synthesis (EdU incorporation) measured when cultured under the conditions shown in (F).

Data are presented as the ratio of nuclei positively labeled for both GFP+EdU relative to total GFP-labeled tumor cell nuclei. Chip data were obtained from analysis of 5–6 regions per chip in 2–3 chips per condition in 3 separate experiments; *$p < 0.05$; ***$p < 0.001$; ns, not significant.

See also Figure S1.

breathing motions on-chip, the tumor cells expanded to replace large regions of the epithelium (Figures 1E, middle, and 1G), and grew both above and below the epithelial layer (Figures 1B and 1G), whereas the same tumor cells remained limited to smaller localized regions of the epithelium when grown with cyclic deformation (Figure 1E, right). This observation raises that possibility

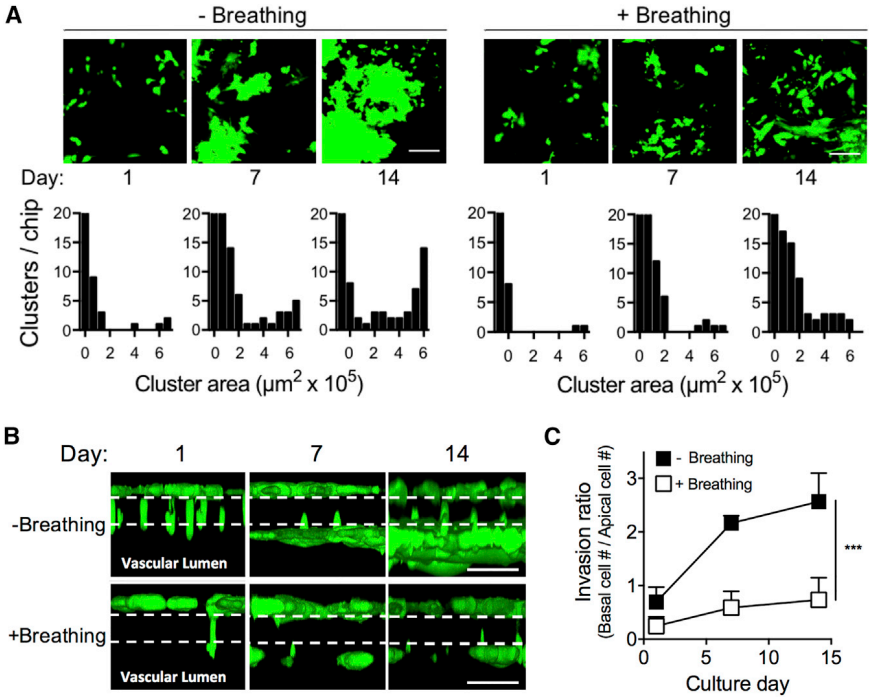

Figure 2. Effects of Mechanical Breathing on Cancer Cell Growth Patterns and Vascular Invasion In Vitro

(A) Fluorescence microscopic images (top) showing GFP-labeled lung cancer cell clusters growing within the epithelium of the alveolus chip cultured for 1, 7, and 14 days in the absence (−Breathing) or presence (+ Breathing) of cyclic mechanical deformations that mimic physiological breathing motions (scale bar, 100 μm). Cluster area histograms (bottom) generated with computerized image analysis confirm that larger cell clusters form in the absence of breathing motions.

(B) High-magnification confocal fluorescence microscopic z-stack images of GFP-labeled NSCLC cells within the breathing and non-breathing alveolar chips presented in a showing that the cancer cells invade from the epithelial channel through the ECM-filled pores of the PDMS membrane (dashed lines) and into the endothelium within vascular channel below and that this process is suppressed when the alveolar chips experience breathing motions (scale bar, 100 μm).

(C) Quantification of the invasive behavior shown in (B).

Data are presented as the ratio of the GFP intensity measured within tumor cells on the lower vascular side of the membrane to the GFP signal within tumor cells above the membrane on the epithelial side (obtained from analysis of 5–6 regions per chip in 2–3 chips per condition in 3 separate experiments; ***$p < 0.001$).

See also Figure S2.

that loss of lung motion due to filling of the alveolar spaces by growing cancer cells or other causes (e.g., airway obstruction) could produce a positive feedback loop to further enhance tumor cell proliferation during disease progression.

Given that rampant tumor cell proliferation is a key contributor to cancer, we next analyzed how the normal lung tissues contribute to this response. To focus on effects independent of fluid flow or breathing motions, we carried out these studies in Transwell inserts. Co-culture with endothelium alone did not significantly support NSCLC cell growth whether measured by quantifying cell number (Figure 1H) or incorporation of 5-ethynyl-2′-deoxyuridine (EdU) into DNA (Figures 1I and S1A). In contrast, co-culture of the tumor cells with lung alveolar epithelial cells dramatically increased their growth, whereas further addition of endothelium significantly ($p < 0.001$) suppressed this response (Figures 1H and 1I). This effect appeared to be mediated by soluble factors as epithelium-conditioned medium produced nearly identical effects on NSCLC growth as co-culture with living cells (Figure S1B). Moreover, the growth suppressing effects of the endothelium seems to be specific for the lung cancer cells since the proliferative rate of the normal epithelium was unaffected by co-culture with endothelium in the absence of cancer cells (Figure S1C).

Effects of Mechanical Breathing on Cancer Behavior

As the migration dynamics and formation of cancer cell clusters have been shown to contribute to the development of the invasive phenotype and resistance to therapy (Zhai et al., 2017), we leveraged our ability to monitor lung cancer cell migration over time within the alveolus chip. Fluorescence microscopic imaging and computerized morphometric analysis of the GFP-labeled NSCLC cells after 14 days of co-culture revealed that larger tumor cell clusters formed in the static alveolus chips compared to the mechanically active breathing Chips (Figure 2A), which is consistent with the differentials in tumor cell growth we observed (Figure 1F, bottom). Importantly, we also were able to visualize active tumor cell migration and invasion through the tissue boundary and ECM that fills the membrane pores separating the epithelium and endothelium (Figures 1B and 2B), which is a unique feature of the alveolus chip. This resulted in accumulation of tumor cells within endothelium and their expansion into the vascular channel over time, observed by confocal microscopy (Figure 2B) or sectioning and histological staining (Figure S2), and again we found that breathing motions suppressed this invasive response by ~50% ($p < 0.001$) (Figures 2B and 2C).

Analysis of Drug Responses in the Orthotopic Lung Cancer Chip Model

The H1975 cell line is derived from a NSCLC tumor that harbors an activating mutation (L858R in exon 21), and a second acquired EGFR point mutation at T790M (Sordella et al., 2004). While NSCLC patients with activating EGFR mutations typically have good initial responses to therapy with first-generation reversible TKIs, such as erlotinib (Sordella et al., 2004; Mok et al., 2009; Rosell et al., 2012), disease progression commonly reoccurs within 9–14 months of therapy in patients who acquire an additional EGFR mutation (e.g., T790M), which is less sensitive to this therapy (Gazdar, 2009; Sequist et al., 2011). In these

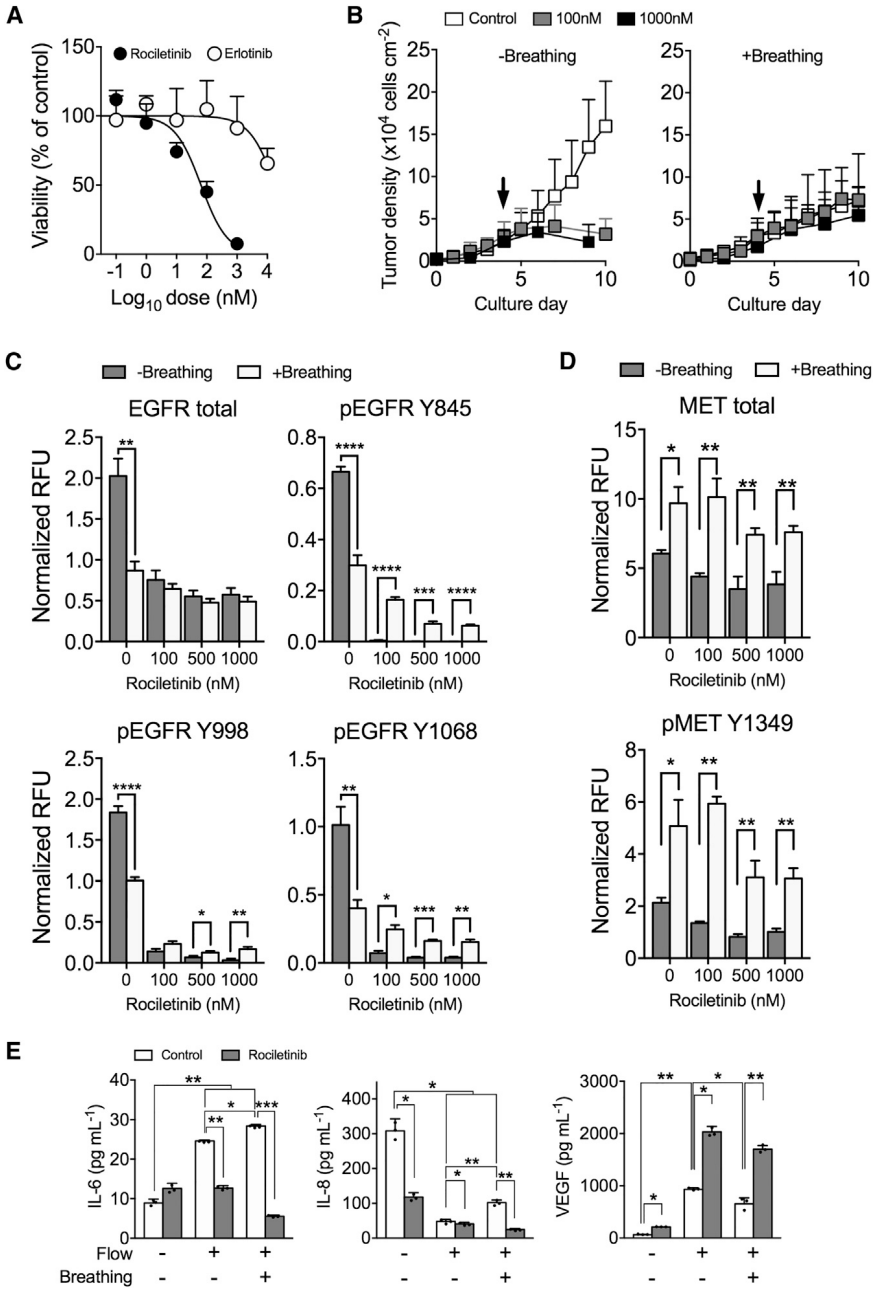

Figure 3. Breathing Modulates Lung Cancer Cell Responses to a TKI Drug

(A) The NSCLC tumor cells, which express EGFR L858R/T790M mutations, show increased sensitivity to the third-generation TKI rociletinib (black circles) compared to first-generation erlotinib (open circles). Data are presented as the number of viable NSCLC cells as a percentage of the number of viable untreated cells (control) measured with the MTS assay after 72 hr of drug exposure (error bars indicated standard deviation; data obtained from 3 wells per condition in 3 separate experiments).

(B) Growth of NSCLC tumor cells in alveolar chips cultured in the presence of 0 (control; open squares), 100 (gray squares), or 1000 nM (black squares) rociletinib (arrow indicates time of drug addition) in the absence (left) or presence (right) of breathing motions. Data were obtained from 5–6 regions per chip in 2–3 chips per condition in 3 separate replica studies.

(C) Total EGFR tyrosine phosphorylation levels (EGFR total) and levels of phosphorylation measured at tyrosine 845 (pEGFR Y845), 998 (pEGFR Y998), and 1068 (pEGFR 1068) in NSCLC tumor cells cultured for 2 days in presence of 0, 100, 500, or 1,000 nM rociletinib for 2 days in the absence (–Breathing; gray) or presence (+Breathing; white) of cyclic mechanical strain (10%; 0.2 Hz). Phosphorylated values are normalized with respect to the corresponding total EGFR. Data were obtained from 2–4 samples in 2 separate experiments; *p < 0.05; **p < 0.01.

(D) Top and bottom graphs respectively show total cMET levels (MET total) and levels of phosphorylation measured at tyrosine 1349 (pMET Y1349) in NSCLC tumor cells cultured for 2 days in the presence of 0, 100, 500 or 1000 nM rociletinib for 2 days in the absence (-Breathing; gray) or presence (+Breathing; white) of cyclic mechanical strain (10%; 0.2 Hz). Phosphorylated values are normalized with respect to the corresponding total MET. Data were obtained from 2–4 samples in 2 separate experiments; *p < 0.05; **p < 0.01.

(E) Production of cytokines, IL-6, IL-8, and VEGF by NSCLC cells, alveolar epithelial cells, and lung endothelial cells co-cultured in Transwells (–Flow, –Breathing) versus the alveolus chip in the absence (+Flow, –Breathing) or presence (+Flow, +Breathing) of cyclic mechanical strain mimicking breathing motions.

Data represent averages from 3–6 chips per experiment in 3 separate experiments; *p < 0.05, **p < 0.01, ***p < 0.001.

cases, treatment with a third-generation irreversible TKI that targets kinases that phosphorylate both sites, such as rociletinib, is recommended (Sequist et al., 2015); yet patients with late-stage NSCLC still often eventually fail to respond to therapy (Thress et al., 2015; Chabon et al., 2016).

We therefore first characterized how the H1975 NSCLC cells respond to first- and third-generation TKIs (erlotinib and rociletinib, respectively) when cultured under different microenvironmental conditions. As expected given their acquired second point mutation, these NSCLC cells are significantly more sensitive to the inhibitory effects of rociletinib than erlotinib (half-maximal inhibition at >1,000 nM versus ~100 nM, respectively) when cultured alone under conventional static culture conditions (Figure 3A). Similarly, when we administered rociletinib at similar doses to lung cancer cells cultured within static alveolus chips, we found again that the tumor was more sensitive to this TKI drug in that complete growth suppression was observed at the lower dose (100 nM; Figure 3B, left). Even more interestingly, these lung cancer cells were almost completely resistant to the inhibitory effects of this third-generation TKI when growing on-chip in the presence of physiological breathing motions (Figure 3B, right).

Modulation of Tyrosine Kinase Activity by Mechanical Strain

The decreased sensitivity of cancer cells to the TKI drug in the breathing alveolus chip could be due to mechanical regulation of EGFR expression and signaling within the tumor cells, and so we cultured the NSCLC cells with or without cyclic mechanical deformation (10% strain; 0.2 Hz) for 48 hr in a FlexCell culture plate to test this hypothesis independent of other lung cells or fluid flow. Mechanical stimulation produced a significant ($p < 0.05$) decrease in total EGFR protein levels in the NSCLC cells even before rociletinib was added (Figure 3C), which could possibly account for the observed inhibitory effects of breathing motions on growth (Figure 1F, bottom) and motility (Figures 2B and 2C). Furthermore, while we found that treatment of these tumor cells with rociletinib resulted in the inhibition of tyrosine kinase phosphorylation at EGFR sites Y845, Y998, and Y1068 in the absence of breathing motions, this inhibition also was greatly diminished in the mechanically stimulated cells (Figure 3C). Thus, both downregulation of EGFR and reduced suppression of phosphorylation of the EGFRs that were expressed could explain why the mechanically strained cells were resistant to growth inhibition by this third-generation TKI drug (Figure 3B, right).

Another important clinical observation is that many patients with the EGFR L858R/T790M mutation who develop resistance to third-generation TKIs overexpress the tyrosine protein kinase c-Met (Finocchiaro et al., 2015; Huang and Fu, 2015; Stewart et al., 2015; Zhao et al., 2015; Chabon et al., 2016; Morgillo et al., 2016), and c-MET overexpression has been implicated as a mechanism of resistance to TKI therapy in NSCLC patients (Sadiq and Salgia, 2013). Consistent with our finding that breathing motions decrease NSCLC cell sensitivity to this TKI, we found that the NSCLC cells significantly increased both their expression and phosphorylation of c-Met when subjected to cyclic mechanical strain, whereas increasing rociletinib dose had no significant effect (Figure 3D). Thus, mechanical breathing motions also may suppress NSCLC cell response to TKI therapy by altering this signaling pathway.

Mechanical and Therapeutic Modulation of Cytokines

Past in vivo studies have revealed that the cytokines, IL-6, IL-8, and VEGF, may serve as clinically important prognostic indicators of cancer growth (Enewold et al., 2009; Junttila and de Sauvage, 2013; Umekawa et al., 2013). Because the alveolus cancer chip model features fluid flow in the vascular channel, we were able to analyze these secreted components within effluents collected over time from this compartment. These studies revealed that IL-6 and VEGF are more abundant, whereas IL-8 was decreased, in the microfluidic alveolar chip model of NSCLC with or without breathing when compared to Transwell cultures without breathing or flow (Figure 3E). In addition, treatment of the lung tumor cells with rociletinib significantly reduced levels of IL-6 and IL-8, and increased VEGF levels in both static and breathing alveolus chips; however, the level of suppression of the two interleukins was significantly greater in chips exposed to physiological breathing motions (Figure 3E). Importantly, the finding that TKI treatment reduces IL-8 levels in our orthotopic in vitro lung cancer model is also consistent with published results from human clinical trials (Enewold et al., 2009; Umekawa et al., 2013).

DISCUSSION

Taken together, these studies revealed that local microenvironmental cues elicited by cells that comprise the epithelial and endothelial tissues of the lung, as well as by mechanical breathing motions, can significantly influence NSCLC growth in vitro. More importantly, these data show that these orthotopic cancer chip models mimic the unique growth patterns that are observed in human patients with the adenocarcinoma form of this lung cancer in vivo (Yousem and Beasley, 2007). Interestingly, many patients with late stage NSCLC who already display T790M mutations eventually develop resistance and fail to respond to therapy with third-generation TKI inhibitors (Thress et al., 2015; Chabon et al., 2016). We were also able to recapitulate development of this new type of resistance by culturing the cancer cells in the orthotopic breathing lung alveolus, but not under conventional static culture conditions. In addition, many patients with the EGFR L858R/T790M mutation who develop resistance to third-generation TKIs overexpress the tyrosine protein kinase c-Met (Finocchiaro et al., 2015; Huang and Fu, 2015; Stewart et al., 2015; Zhao et al., 2015; Chabon et al., 2016; Morgillo et al., 2016), and again, the human orthotopic lung chip culture environment that promoted resistance to TKI therapy increased both the expression and phosphorylation of c-Met. Our finding that TKI treatment reduces IL-8 levels in the breathing lung alveolus cancer chip in vitro is also consistent with published results from human clinical trials (Enewold et al., 2009; Umekawa et al., 2013), and this has not been previously replicated using conventional culture models.

The ability to maintain these H1975 human cancer cells in an organ-relevant microenvironment in a non-growing, dormant state is unusual as well, and potentially valuable, given that tumor dormancy and the presence of cancer persister cells are some of the key challenges that must be overcome to prevent cancer recurrence in patients in remission or with residual disease (Holmgren et al., 1995; Ramirez et al., 2016). This is an important observation for the lung cancer field because the H1975 NSCLC cell line is often used by the pharmaceutical industry in their efforts to discover new TKI drugs and other therapeutics for treatment of NSCLC. This finding that breathing motions suppress NCSLC cell responses to therapy also offers a potential explanation for why it is so difficult to eradicate minimal residual disease which appears within functional (aerated) parts of the lung after larger (alveolar space-filling) NSCLC tumors are induced to regress by treatment with TKI drugs in patients. Discovery of this previously unappreciated mechanism for developing resistance to therapy could help to lead to development of new forms of drug resistance mitigation, if future experiments validate this mechanism in vivo.

In conclusion, these results demonstrate that microfluidic organ chip technology can be used to create in vitro human orthotopic lung cancer models that faithfully mimic microenvironment-specific growth patterns, cytokine secretion profiles, and clinical responses to therapy previously observed in human patients, as well as permit analysis of molecular level modulation of

drug actions by the organ microenvironment, which has not been previously possible with other in vitro cancer models or even with animal studies. One potential limitation of this model is that it does not contain tumor stromal cells or immune cells; however, these cells and virtually any other relevant type of cell could be integrated into these cancer chips in the future. The more important observation is that because organ chips utilize a bottom-up, synthetic biology approach, our results indicate that these other cell types are not required for expression of the NSCLC phenotypes we recapitulated here as the combined presence of lung epithelium, endothelium and breathing motions is sufficient to manifest these behaviors. The ultimate value of these human orthotopic cancer chip models lies in their potential ability to uncover new insights into mechanisms of cancer control, and to facilitate discovery of novel drug targets and anti-cancer therapeutics.

EXPERIMENTAL PROCEDURES

Device Fabrication

Our methods for fabricating the organ chips have been previously described (Huh et al., 2010, 2012; Benam et al., 2016a, 2016b). In brief, the upper and lower layers of the microfluidic device (Figure 1C) were created by casting polydimethylsiloxane (PDMS) pre-polymer on molds prepared using stereo-lithography (Fineline, USA). Curing (10:1 PDMS base to curing agent, wt/wt %) was carried out overnight at 60°C to produce devices containing two adjacent parallel microchannels (top channel, 1,000-μm wide × 1,000-μm high; bottom channel, 1,000-μm wide × 200-μm high; length of overlapping channels, 16.7 mm), which were used to form the air-filled lumen and the microvascular channel, respectively. The channels were separated by a thin (~10 μm) semi-porous polyester (polyethylene terephthalate [PET]) membrane (0.4-μm pores; Maine Manufacturing, USA) in the airway chip, or a PDMS membrane (25- to 50-μm thick; 9-μm pores) in the alveolus chip, which was made in house.

Cell Culture

Human primary airway epithelial cells (Lonza, USA) were cultured as previously described (Benam et al., 2016a, 2016b). Primary human primary alveolar epithelial cells and human lung microvascular endothelial cells (both from Cell Biologics, USA) were expanded in gelatin-coated tissue culture flasks using complete epithelial cell growth medium or endothelial cell growth medium, respectively, obtained from the same supplier. H1975 NSCLC tumor cells (ATTC) that were used in these studies were infected with lentivirus containing the transgene integration, (CMV) → Luciferase (SV40) → eGFP-IRES-puro (GeneCopoeia), according to manufacturer's protocol with 5 μg/mL polybrene at 4°C for 1 hr. Puromycin (1 μM) was included in tumor cell cultures for 2–3 passages, after which the cancer cells exhibited stable high levels of GFP expression for multiple passages (>1 month), as confirmed by flow cytometry.

Transwell inserts with polyester-PET membranes (6.5-mm diameter, 0.4-μm pore; Corning, USA) were plasma treated for 1 min in an Atto Plasma Cleaner (Diener, Germany) before being coated with a mixture of human ECM proteins containing laminin (0.5 mg/mL; Sigma), fibronectin (1 mg/mL; Akron), and collagen type I (3.2 mg/mL; Advanced Biomatrix) for at least 2 hr at room temperature. The inserts were gently aspirated and washed with medium prior to plating the cells. For co-culture experiments, the Transwell inserts were first flipped upside-down in a sterile petri dish lid, seeded with endothelial cells at high density (6.4 × 10^5 cells in 35-μl endothelial growth medium; 2 × 10^6 cm^{-2}), allowed to attach in a CO_2 incubator at 37°C for 1 hr, and then flipped right-side up and returned to well plates containing 500 μL endothelial growth medium in each basal chamber. Next, GFP-labeled NSCLC cells were plated in the apical chamber (1,024 cells in 100 μL epithelial growth medium; 3.2 × 10^3 cm^{-2}) for 3 hr before alveolar epithelial cells were added to the same upper chamber (6.4 × 10^4 cells in 200 μL epithelial growth medium; 2 × 10^5 cm^{-2}). After culture overnight in a CO_2 incubator at 37°C, the apical medium was replaced with the same medium containing 1 μM dexamethasone to promote surfactant production and formation of tight junctions (Huh et al., 2010). The apical liquid was removed 2–3 days later to create an ALI; thereafter, the epithelial cells were fed only by an ALI medium within the basal chamber (400 μL per well), which was composed of endothelial basal medium and supplements (Cell Biologics) with reduced fetal bovine serum (0.4%), EGF (0.01%), and additional $CaCl_2$ (1 μM), but without phenol red or endothelial cell growth supplement (ECGS) (FGF). This medium was optimized to support long-term survival of the primary alveolar epithelium and endothelium under these conditions.

Microfluidic Organ Chip Culture

The methods for carrying out lung airway and alveolus chip cell culture studies have been described previously (Huh et al., 2010, 2012; Benam et al., 2016a, 2016b; Jain et al., 2017). For the small airway chip studies, the PDMS microfluidic chips with PET membranes were plasma treated and coated with ECM using the same method used to coat the Transwell PET membranes. The GFP-labeled NSCLC cells were then injected with a syringe into the upper channel of the chip (530 cells in 35 μl epithelial growth medium; 3.2 × 10^3 cells cm^{-2}) and allowed to attach for 3 hr under static conditions at 37°C before the medium was removed gently with a syringe and primary small airway epithelial cells were injected (3.3 × 10^4 cells in 35 μL epithelial growth medium; 2 × 10^5 cells cm^{-2}) into the same channel. The chips were cultured statically and the medium was gently removed and replaced with a syringe once every day; after 3 days, the medium was removed from the apical channel to create an ALI, and ALI medium supplemented with 50 ng/mL retinoic acid (Benam et al., 2016a, 2016b) was then perfused through the basal channel (60 μL hr^{-1}) driven by a peristaltic pump (ISM 933, ISMATEC, Germany). After the airway epithelial cells were allowed to differentiate for approximately 2 weeks, the chips were taken off flow, primary human lung microvascular endothelial cells were seeded in the basal channel of the microfluidic device (3.3 × 10^5 cells in 35 μL; 2 × 10^6 cell cm^{-2}), and the devices were flipped upside-down and cultured in an incubator for 2 hr under static conditions before being returned to their normal orientation for another hour to ensure endothelial cell coverage of all four walls of the lower channel. Chips were then reconnected to the peristaltic pump and perfused (60 μL hr^{-1}) through the lower vascular channel for the remainder of the experiment.

In the experiment in which cancer cells were implanted into pre-differentiated airway chips, the GFP-labeled NSCLC cells were loaded (10^4 cells mL^{-1}) in a syringe with 29 gauge needle tip, inserted through the PDMS, and injected into the differentiated layer of normal airway epithelium on the top surface of the porous membrane within the chip, while viewing under a bright-field microscope. This was repeated until several localized areas of GFP-labeled cancer cells successfully integrated into the epithelium.

For the alveolar chip studies, PDMS microfluidic chips with PDMS membranes were plasma treated, then immediately exposed to 10% APTMS (aminopropyltrimethsiloxane) in pure ethanol for 10 min, washed 3 times with ethanol, dried in an 80°C oven overnight, and then coated with the same ECM mixture used for the Transwell inserts. The primary human lung microvascular endothelial cells were plated the same way as in the airway chips, except that these cells were plated first with endothelial growth medium. The GFP-labeled NSCLC tumor cells and primary alveolar epithelial cells were then plated using the same method as described for the airway chips. The following day, the apical channel was perfused with epithelial growth medium containing 1 μM dexamethasone and flushed manually for 2–3 days, after which, the medium in the apical channel was removed to create an ALI, while the basal channel of the chip was continuously perfused with ALI medium via peristaltic flow (60 μL hr^{-1}). In studies in which physiological breathing motions were mimicked, cyclic strain (10% strain, 0.2 Hz) was initiated 3 days after the creation of the ALI by applying vacuum (−75 kPa) to the hollow side chambers of the device, as previously described (Huh et al., 2010, 2012).

Cancer Cell Growth Monitoring

Tumor cell growth was monitored non-invasively on-chip and in the Transwell cultures using fluorescence microscopy every 1–2 days, and the number of GFP-labeled cells was estimated based on a standard curve generated experimentally that correlate cell density to GFP fluorescence intensity. In parallel studies, we quantified DNA synthesis within the tumor cells by adding EdU (EdU Click-iT Plus LifeTechnologies) to the culture medium for 24 hr prior to fixation. For conditioned medium studies, tumor cells were seeded in complete

growth medium in wells of a 96-well plate at the same density as co-culture experiments (3.2×10^3 cells cm^{-2}) and allowed to attach overnight. The medium (100 μL per well) was then replaced daily with conditioned medium that had been removed from basal chambers of Transwells in which human alveolar epithelial cells had been cultured alone in the top chamber of the insert.

For the monoculture TKI studies, stock solutions of erlotinib and rociletinib (both from Cayman Chemicals) were dissolved in DMSO and then diluted in complete growth medium (final concentration of 0.1% DMSO in all samples). The tumor cells were plated at 1,024 cells per well (3.2×10^3 cells/cm^2) in 96-well plates, allowed to attach overnight, and then exposed to indicated concentrations of the TKIs in the complete growth medium for 72 hr. The number of viable cells was quantified using an MTT/MTS CellTiter 96 AQueous One Solution Cell Proliferation Assay (Promega) and by measuring absorbance at 490 nm; data are reported as the percentage of viable cells with respect to the 0.1% DMSO vehicle condition. For drug studies on-chip, ALI medium with or without different concentrations of rociletinib was continually perfused (60 μL/hr^{-1}) through the basal vascular channel beginning 1 day after initiation of cyclic mechanical strain application.

Morphological Analysis, Computerized Morphometry, and Histology

For live-cell GFP imaging, organ chips and Transwell cultures were imaged using confocal laser-scanning microscopy system (Leica SP5 X MP) with HybriD detector and a Ludin incubation chamber with active CO_2 control to maintain the samples at optimal temperature, CO_2, and humidity or a Zeiss Axio Observer Z1 microscope with Hamamatsu 9100-02 EMCCD. For immunostaining studies, Transwells and organ chips were washed with PBS, fixed with 4% paraformaldehyde (Electron Microscopy Sciences, USA), washed with PBS, permeabilized with 0.2% Triton X-100 (Sigma) in PBS, and blocked with PBS containing 2% BSA (Sigma) prior to incubating samples with antibodies directed against GFP (Abcam ab5450), ZO1 (Life Technologies 617300), and VE-cadherin (Life Technologies 19612) to visualize cancer cells, epithelial tight junctions, and endothelial cell-cell adhesions, respectively. Primary antibodies diluted in blocking buffer were introduced into the apical and basal microchannels of the organ chips and incubated at room temperature for at least 2 hr, replacing the primary antibody solutions every 30 min to account for the small volumes. After washing 3 times with PBS at room temperature, the samples were then incubated with secondary antibodies for an additional 1 hr at room temperature, followed by counterstaining with 1:1,000 Hoechst in PBS for 10 min to visualize nuclei, and washing in PBS. The membranes with fixed, and stained adherent cells were then cut free from the chip and mounted on microscopy slides in Prolong Diamond Antifade Mountant (Life Technologies, P36961). Fluorescence imaging was carried out using a Zeiss TIRF/LSM 710 confocal microscopy and Hamamatsu ImagEM-1K BackThinned EMCCD camera. Image processing and 3D z-stack reconstruction were done using Imaris (Bitplane, Switzerland) and ImageJ/FIJI software (https://imagej.net/Fiji).

For analysis of the size and distribution of cancer clusters on chip, epifluorescent images were analyzed in FIJI using the built-in Analyze Particles software. The particle area distributions were then imported to MATLAB (MathWorks, USA) and analyzed using the statistics toolbox for optimized histogram binning. Invasion quantification from Figure 2C was done using the confocal z stacks from Figure 2B; image stacks were imported into FIJI, where each stack was manually divided into above and below the PDMS membrane. Thresholds were applied to the resulting sub-stacks and summed for GFP-labeled areas.

For histological staining, we used a modified version of a previously published rapid histology method (Elfer et al., 2016) in which organ chips were fixed in 4% paraformaldehyde/0.1% glutaraldehyde in PBS for 1 hr at room temperature, incubated with H&E-Y (0.5%) in water for 10 min at room temperature, and then sectioned by hand with a scalpel and imaged using confocal light microscopy.

Cytokine Analysis

To compare cytokines secreted by cells cultured within alveolus chips with or without breathing versus in Transwell inserts, medium samples (400 μL) were collected every day from the basal chamber of the Transwells and every other day from the outflow of the lower vascular channel of the chips to account for the twice larger surface area of the Transwells (0.32 cm^2 versus 0.167 cm^2 for each channel of the chips), and then frozen and stored at −80°C. Thawed effluent samples were diluted according to manufactures guidelines (1:2 or 1:10 depending on cytokine) and multiplexed cytokine measurements for VEGF, IL-6, and IL-8 were performed using an electrochemilluminescence immunoassay (Meso Scale Discovery, Rockville, MD, USA) on a QuickPlex SQ 120 instrument.

EGFR Phosphorylation Analysis

The NSCLC tumor cells were plated (~1×10^6 cell per well) in complete growth medium on collagen I-coated flexible 6-well plates (BioFlex Culture Plate; Flexcell Intel Corporation, Burlington, NC, USA). The next day, the medium was replaced with ALI medium containing 0, 100, 500, or 1,000 nM rociletinib. Cyclic mechanical deformation (10% strain; 0.2 Hz) was applied using the BioFlex baseplate with loading stations and FX5K Tension FlexLink to mimic breathing motions, and 2 days later, cells were lysed on ice using cell lysis buffer supplemented with 1 mM phenylmethylsulfonyl fluoride (both from Cell Signaling Technologies, USA). Lysates were centrifuged at 4°C, and the supernatants were collected and transferred to array slides from the PathScan EGFR Signaling Antibody Array Kit (Fluorescent Readout; Cell Signaling Technologies). Antibody array slides were incubated with the lysate overnight at 4°C, followed by primary and secondary staining, and imaged using a Zeiss Axio Observer Z1 with Hamamatsu Orca-Flash 4.0 sCMOS camera. Fluorescence intensity of each microdot was quantified using ImageJ software, first applying a uniform threshold, then calculating the integrated fluorescent intensity and lastly normalizing to the housekeeping protein on each assay pad array.

Statistical Analysis

All results and error bars are presented as mean and SEM unless otherwise noted. Data were analyzed with an unpaired Student's t test using GraphPad Prism (GraphPad Software, San Diego, CA, USA) software. Differences between groups were considered statistically significant when $p < 0.05$.

SUPPLEMENTAL INFORMATION

Supplemental Information includes two figures and can be found with this article online at https://doi.org/10.1016/j.celrep.2017.09.043.

AUTHOR CONTRIBUTIONS

B.A.H. and D.E.I. conceived and designed the studies; B.A.H. and G.G. developed the basic cancer chip model and methods; B.A.H. optimized and conducted cancer chip studies and all imaging; E.L. and C.S.C. helped design and perform the EGFR-phosphorylation experiments; A.S.-P. and B.A.H. performed the chip sectioning and histology; B.A.H., G.G., O.L., and D.E.I. prepared the manuscript and illustrations; and all authors critically revised the manuscript.

ACKNOWLEDGMENTS

This research was supported by the Wyss Institute for Biologically Inspired Engineering at Harvard University and the Defense Advanced Research Projects Agency (DARPA) (under cooperative agreement number W911NF-12-2-0036) (to D.E.I); an International Foundation for Ethical Research (IFER) graduate fellowship (to B.H.); and an LE&RN postdoctoral grant from the Lymphatic Education and Research Network and a BU-CTSI grant (TL1TR001410) from the National Center for Advancing Translational Sciences at the NIH (to E.L.). The views and conclusions contained in this document are those of the authors and should not be interpreted as representing the official policies, either expressed or implied, of DARPA or the U.S. Government. The authors also thank T. Ferrante, K. DeGouveia, and D. Chou for technical assistance; E. Benecchi (Harvard Medical School Electron Microscopy Facility) for assistance with histological sectioning; and L. Jin for her artwork. D.E.I. holds equity in Emulate, Inc., consults to the company, and chairs its scientific advisory board.

Received: June 21, 2017
Revised: August 22, 2017
Accepted: September 12, 2017
Published: October 10, 2017

REFERENCES

Benam, B.K.H., Novak, R., Nawroth, J., Hirano-kobayashi, M., Ferrante, T.C., Choe, Y., Prantil-baun, R., James, C., Bahinski, A., Parker, K.K., and Ingber, D.E. (2016a). Matched-comparative modeling of normal and diseased human airway responses using a microengineered breathing lung chip. Cell Syst. *5*, 456–466.e4.

Benam, K.H., Villenave, R., Lucchesi, C., Varone, A., Hubeau, C., Lee, H.-H., Alves, S.E., Salmon, M., Ferrante, T.C., Weaver, J.C., et al. (2016b). Small airway-on-a-chip enables analysis of human lung inflammation and drug responses in vitro. Nat. Methods *13*, 151–157.

Bhatia, S.N., and Ingber, D.E. (2014). Microfluidic organs-on-chips. Nat. Biotechnol. *32*, 760–772.

Chabon, J.J., Simmons, A.D., Lovejoy, A.F., Esfahani, M.S., Newman, A.M., Haringsma, H.J., Kurtz, D.M., Stehr, H., Scherer, F., Karlovich, C.A., et al. (2016). Circulating tumour DNA profiling reveals heterogeneity of EGFR inhibitor resistance mechanisms in lung cancer patients. Nat. Commun. *7*, 11815.

Choi, Y., Hyun, E., Seo, J., Blundell, C., Kim, H.C., Lee, E., Lee, S.H., Moon, A., Moon, W.K., and Huh, D. (2015). A microengineered pathophysiological model of early-stage breast cancer. Lab Chip *15*, 3350–3357.

Elfer, K.N., Sholl, A.B., Wang, M., Tulman, D.B., Mandava, S.H., Lee, B.R., and Brown, J.Q. (2016). 'DRAQ5 and eosin ('D&E') as an analog to hematoxylin and eosin for rapid fluorescence histology of fresh tissues. PLoS One *11*, e0165530.

Enewold, L., Mechanic, L.E., Bowman, E.D., Zheng, Y.-L.L., Yu, Z., Trivers, G., Alberg, A.J., and Harris, C.C. (2009). Serum concentrations of cytokines and lung cancer survival in African Americans and Caucasians. Cancer Epidemiol. Biomarkers Prev. *18*, 215–222.

Fidler, I.J., Wilmanns, C., Staroselsky, A., Radinsky, R., Dong, Z., and Fan, D. (1994). Modulation of tumor cell response to chemotherapy by the organ environment. Cancer Metastasis Rev. *13*, 209–222.

Finocchiaro, G., Toschi, L., Gianoncelli, L., Baretti, M., and Santoro, A. (2015). Prognostic and predictive value of MET deregulation in non-small cell lung cancer. Ann. Transl. Med. *3*, 83.

Gazdar, A.F. (2009). Activating and resistance mutations of EGFR in non-small-cell lung cancer: role in clinical response to EGFR tyrosine kinase inhibitors. Oncogene *28* (*Suppl 1*), S24–S31.

Gould, S.E., Junttila, M.R., and de Sauvage, F.J. (2015). Translational value of mouse models in oncology drug development. Nat. Med. *21*, 431–439.

Hackam, D.G., and Redelmeier, D.A. (2006). Translation of research evidence from animals to humans. JAMA *296*, 1731–1732.

Holmgren, L., O'Reilly, M.S., and Folkman, J. (1995). Dormancy of micrometastases: balanced proliferation and apoptosis in the presence of angiogenesis suppression. Nat. Med. *1*, 149–153.

Huang, L., and Fu, L. (2015). Mechanisms of resistance to EGFR tyrosine kinase inhibitors. Acta Pharm. Sin. B *5*, 390–401.

Huh, D., Matthews, B.D., Mammoto, A., Montoya-Zavala, M., Hsin, H.Y., and Ingber, D.E. (2010). Reconstituting organ-level lung functions on a chip. Science *328*, 1662–1668.

Huh, D., Leslie, D.C., Matthews, B.D., Fraser, J.P., Jurek, S., Hamilton, G.A., Thorneloe, K.S., McAlexander, M.A., and Ingber, D.E. (2012). A human disease model of drug toxicity-induced pulmonary edema in a lung-on-a-chip microdevice. Sci. Transl. Med. *4*, 159ra147.

Jain, A., Barrile, R., van der Meer, A.D., Mammoto, A., Mammoto, T., De Ceunynck, K., Aisiku, O., Otieno, M.A., Louden, C.S., Hamilton, G.A., et al. (2017). A primary human lung alveolus-on-a-chip model of intravascular thrombosis for assessment of therapeutics. Clin. Pharmacol. Ther. Published online May 17, 2017. https://doi.org/10.1002/cpt.742.

Junttila, M.R., and de Sauvage, F.J. (2013). Influence of tumour micro-environment heterogeneity on therapeutic response. Nature *501*, 346–354.

Killion, J.J., Radinsky, R., and Fidler, I.J. (1999). Orthotopic models are necessary to predict therapy of transplantable tumors in mice. Cancer Metastasis Rev. *17*, 279–284.

Mok, T.S., Wu, Y.L., Thongprasert, S., Yang, C.H., Chu, D.T., Saijo, N., Sunpaweravong, P., Han, B., Margono, B., Ichinose, Y., et al. (2009). Gefitinib or carboplatin-paclitaxel in pulmonary adenocarcinoma. N. Engl. J. Med. *361*, 947–957.

Morgillo, F., Della Corte, C.M., Fasano, M., and Ciardiello, F. (2016). Mechanisms of resistance to EGFR-targeted drugs: lung cancer. ESMO Open *1*, e000060.

Pao, W., and Chmielecki, J. (2010). Rational, biologically based treatment of EGFR-mutant non-small-cell lung cancer. Nat. Rev. Cancer. *10*, 760–774.

Portillo-Lara, R., and Annabi, N. (2016). Microengineered cancer-on-a-chip platforms to study the metastatic microenvironment. Lab Chip *16*, 4063–4081.

Ramirez, M., Rajaram, S., Steininger, R.J., Osipchuk, D., Roth, M.A., Morinishi, L.S., Evans, L., Ji, W., Hsu, C., Thurley, K., et al. (2016). Diverse drug-resistance mechanisms can emerge from drug-tolerant cancer persister cells. Nat. Commun. *7*, 10690.

Rosell, R., Carcereny, E., Gervais, R., Vergnenegre, A., Massuti, B., Felip, E., Palmero, R., Garcia-Gomez, R., Pallares, C., Sanchez, J.M., et al.; Spanish Lung Cancer Group in collaboration with Groupe Français de Pneumo-Cancérologie and Associazione Italiana Oncologia Toracica (2012). Erlotinib versus standard chemotherapy as first-line treatment for European patients with advanced EGFR mutation-positive non-small-cell lung cancer (EURTAC): a multicentre, open-label, randomised phase 3 trial. Lancet Oncol. *13*, 239–246.

Sadiq, A.A., and Salgia, R. (2013). MET as a possible target for non-small-cell lung cancer. J. Clin. Oncol. *31*, 1089–1096.

Sequist, L.V., Waltman, B.A., Dias-Santagata, D., Digumarthy, S., Turke, A.B., Fidias, P., Bergethon, K., Shaw, A.T., Gettinger, S., Cosper, A.K., et al. (2011). Genotypic and histological evolution of lung cancers acquiring resistance to EGFR inhibitors. Sci. Transl. Med. *3*, 75ra26.

Sequist, L.V., Soria, J.-C., Goldman, J.W., Wakelee, H.A., Gadgeel, S.M., Varga, A., Papadimitrakopoulou, V., Solomon, B.J., Oxnard, G.R., Dziadziuszko, R., et al. (2015). Rociletinib in EGFR-mutated non-small-cell lung cancer. N. Engl. J. Med. *372*, 1700–1709.

Siegel, R.L., Miller, K.D., and Jemal, A. (2017). Cancer statistics, 2017. CA Cancer J. Clin. *67*, 7–30.

Skardal, A., Devarasetty, M., Rodman, C., Atala, A., and Soker, S. (2015). Liver-tumor hybrid organoids for modeling tumor growth and drug response in vitro. Ann. Biomed. Eng. *43*, 2361–2373.

Sordella, R., Bell, D.W., Haber, D.A., and Settleman, J. (2004). Gefitinib-sensitizing EGFR mutations in lung cancer activate anti-apoptotic pathways. Science *305*, 1163–1167.

Stewart, E.L., Tan, S.Z., Liu, G., and Tsao, M.S. (2015). Known and putative mechanisms of resistance to EGFR targeted therapies in NSCLC patients with EGFR mutations-a review. Transl. Lung Cancer Res. *4*, 67–81.

Thress, K.S., Paweletz, C.P., Felip, E., Cho, B.C., Stetson, D., Dougherty, B., Lai, Z., Markovets, A., Vivancos, A., Kuang, Y., et al. (2015). Acquired EGFR C797S mutation mediates resistance to AZD9291 in non-small cell lung cancer harboring EGFR T790M. Nat. Med. *21*, 560–562.

Umekawa, K., Kimura, T., Kudoh, S., Suzumura, T., Oka, T., Nagata, M., Mitsuoka, S., Matsuura, K., Nakai, T., Yoshimura, N., et al. (2013). Plasma RANTES, IL-10, and IL-8 levels in non-small-cell lung cancer patients treated with EGFR-TKIs. BMC Res. Notes *6*, 139.

Yousem, S.A., and Beasley, M.B. (2007). Bronchioloalveolar carcinoma: a review of current concepts and evolving issues. Arch. Pathol. Lab. Med. *131*, 1027–1032.

Zhai, W., Lim, T.K., Zhang, T., Phang, S., Tiang, Z., Guan, P., Ng, M., Lim, J.Q., Yao, F., Li, Z., et al. (2017). The spatial organization of intra-tumour heterogeneity and evolutionary trajectories of metastases in hepatocellular carcinoma. Nat. Commun. *8*, 4565.

Zhao, B.X., Wang, J., Song, B., Wei, H., Lv, W.P., Tian, L.M., Li, M., and Lv, S. (2015). Establishment and biological characteristics of acquired gefitinib resistance in cell line NCI-H1975/gefinitib-resistant with epidermal growth factor receptor T790M mutation. Mol. Med. Rep. *11*, 2767–2774.

Cell Reports, Volume *21*

Supplemental Information

Human Organ Chip Models Recapitulate Orthotopic Lung Cancer Growth, Therapeutic Responses, and Tumor Dormancy In Vitro

Bryan A. Hassell, Girija Goyal, Esak Lee, Alexandra Sontheimer-Phelps, Oren Levy, Christopher S. Chen, and Donald E. Ingber

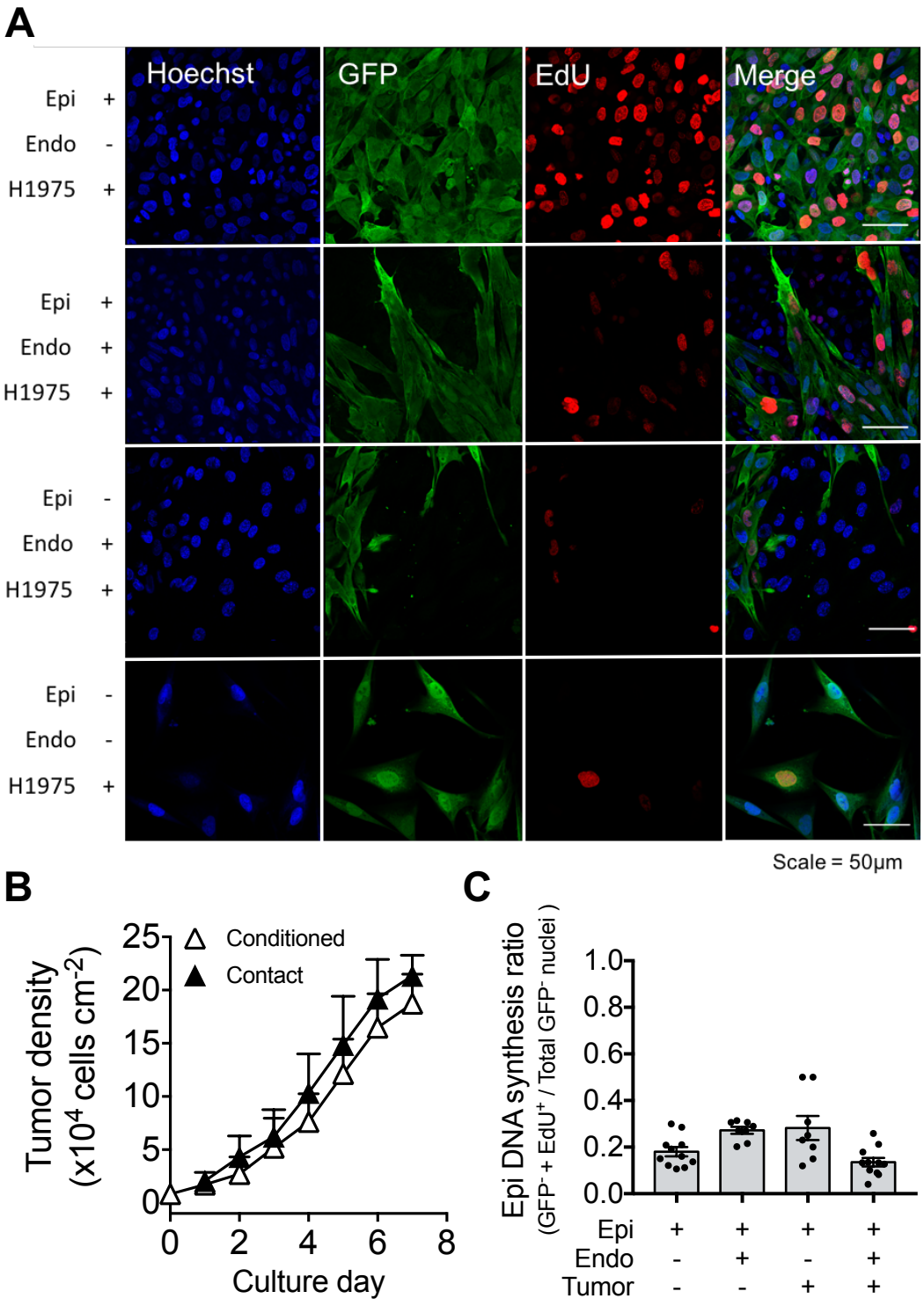

Figure S1. Effects of healthy lung cells on NSCLC tumor cell growth. Related to Fig. 1.
(**A**) Fluorescence microscopic images of GFP-labeled H1975 tumor cells (H1975) cultured in the presence of EdU to quantify DNA synthesis (EdU) either alone or in the presence of alveolar epithelium (Epi) or lung endothelium (Endo) or both in Transwell inserts; Hoechst-stained nuclei and merged images are also shown. (**B**) The NSCLC tumor cells grow equally rapidly when cultured in the presence of conditioned medium from the healthy alveolar epithelial cell cultures (Conditioned) as they do when in direct contact with the epithelial cells (Contact). (C) The growth of alveolar epithelial cells is not significantly altered by co-culture with lung microvascular endothelium, NSCLC tumor cells or both. Data were obtained 3-4 Transwell inserts per condition in 3 separate experiments; there were no significant differences between the conditions, as determined using an unpaired Student's t-test.

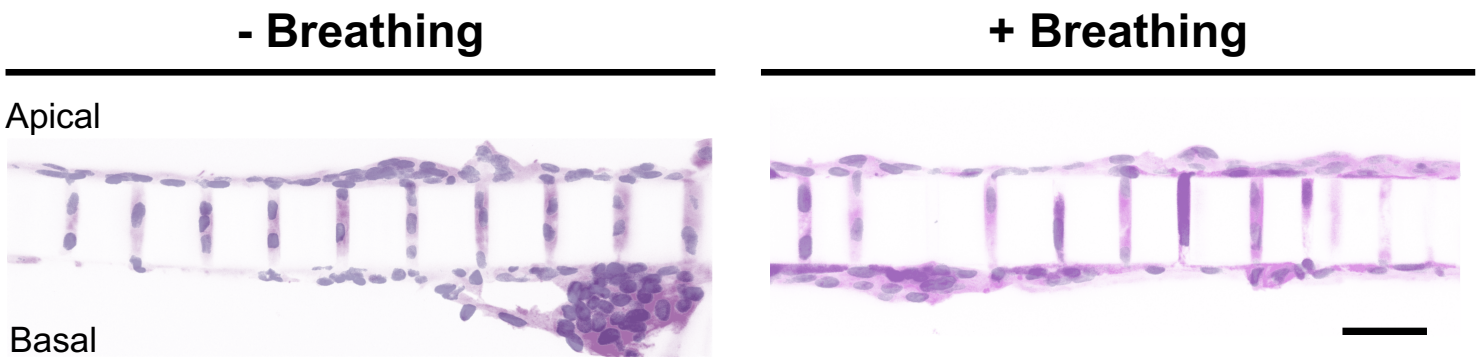

Figure S2. Lung Cancer Chip Histology. Related to Fig. 2. Hematoxylin and Eosin (H&E)-stained vertical sections of the breathing and non-breathing Lung Alveolus Chips in which NSCLC cells were co-plated with normal human lung alveolar epithelial cells in the apical channel on the top surface of the central porous, ECM-coated PDMS membrane and normal human endothelial cells were cultured on the opposite side of the same membrane in the lower channel. The images shown are from Chips that were cultured for 10 days, with or without cyclic breathing motions applied for the last 7 days of culture (bar, 25 μm). Note tumor cells with elongated nuclei migrating (invading) from the apical to basal channels through the vertical pores of the PDMS membrane, as well as increased numbers of tumor cells in the lower channel in the non-breathing Lung Chip (left) compared to breathing Chip (right).